ACSNANO
www.acsnano.org
ARTICLE

Opportunities and Limitations for Nanophotonic Structures To Exceed the Shockley–Queisser Limit

Sander A. Mann,[†] Richard R. Grote,[‡,∥] Richard M. Osgood, Jr.,[‡] Andrea Alù,[§] and Erik C. Garnett*[,†]

[†]Center for Nanophotonics, FOM Institute AMOLF, Science Park 104, 1098 XG Amsterdam, The Netherlands
[‡]Department of Electrical Engineering, Columbia University, 500 W. 120th Street, New York, New York 10027, United States
[§]Department of Electrical and Computer Engineering, The University of Texas at Austin, 1616 Guadalupe St., Austin, Texas 78701, United States

ABSTRACT: **Nanophotonic engineering holds great promise for photovoltaics, with several recently proposed approaches that have enabled efficiencies close to the Shockley–Queisser limit. Here, we theoretically demonstrate that suitably designed nanophotonic structures may be able to surpass the 1 sun Shockley–Queisser limit by utilizing tailored directivity of the scattering response of nanoparticles. We show that large absorption cross sections do not play a significant role in the efficiency enhancement, and on the contrary, directivity enhancement constitutes the nanoscale equivalent to concentration in macroscopic photovoltaic systems. Based on this principle, we discuss fundamental limits to the efficiency based on directivity bounds and a number of approaches to get close to these limits. We also highlight that, in practice, achieving efficiencies above the Shockley–Queisser limit is strongly hindered by whether high short-circuit currents can be maintained. Finally, we discuss how our results are affected by the presence of significant nonradiative recombination, in which case both directivity and photon escape probability should be increased to achieve voltage enhancement.**

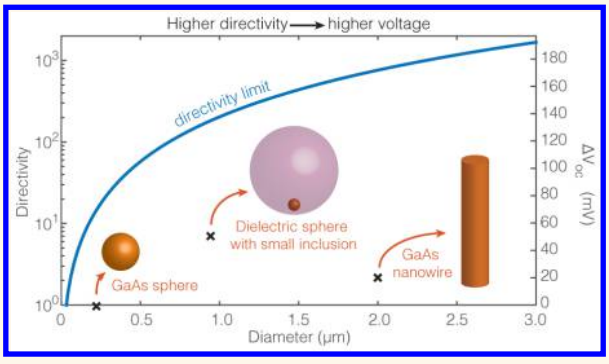

KEYWORDS: *nanophotonics, detailed balance, Shockley–Queisser, open-circuit voltage, photovoltaics, nanowires, efficiency*

Shockley and Queisser showed that the limiting power conversion efficiency of a solar cell can be calculated using the principle of detailed balance.[1] For a single junction solar cell, this limit strongly depends on the semiconductor band gap, and under terrestrial conditions, it peaks at 33.6%. The detailed balance limit is entirely concerned with absorption and emission of photons, both of which can be controlled through nanophotonic engineering. As a result, there has been significant interest in applying nanophotonic concepts to approach or even exceed the Shockley–Queisser limit. Nanophotonics approaches have been studied to enhance the absorption in thin semiconductor layers based on light trapping,[2−15] but more recently, interest has surged in applying nanophotonics to enhance the induced open-circuit voltage in a photovoltaic cell.[16−26] For instance, it is possible to use nanostructures to artificially shift the semiconductor bandgap to higher photon energies[18,19,22,23] or to split the solar spectrum in multijunction solar cells by interlacing detuned nanostructures with large absorption cross sections.[24,25] However, the most promising route to high voltages and efficiencies in single junction solar cells is through concentration (enhancing the short-circuit current relative to the dark current), which increases the maximum efficiency from 33.6% to 45.1%. In macroscopic solar cells this is typically achieved with a concentrating lens (Figure 1a), which focuses the incident sunlight into a much smaller active device area, or by using angle restrictive filters,[8,27−30] which enhance photon recycling (Figure 1b).

In this article, we discuss whether and how nanostructures can enable efficiencies exceeding the 1 sun Shockley–Queisser limit by enhancing the open-circuit voltage (hereafter simply referred to as the SQ limit). For both macroscopic concentration and angle restriction approaches, nanophotonic analogues have been proposed: nanostructures can absorb light from an area much larger than their own size (Figure 1c), and they can provide asymmetric absorption and emission patterns (Figure 1d). Here, we emphasize that only anisotropy in the absorption pattern can lead to efficiencies exceeding the SQ

Received: June 15, 2016
Accepted: August 31, 2016
Published: August 31, 2016

DOI: 10.1021/acsnano.6b03950
ACS Nano 2016, 10, 8620–8631

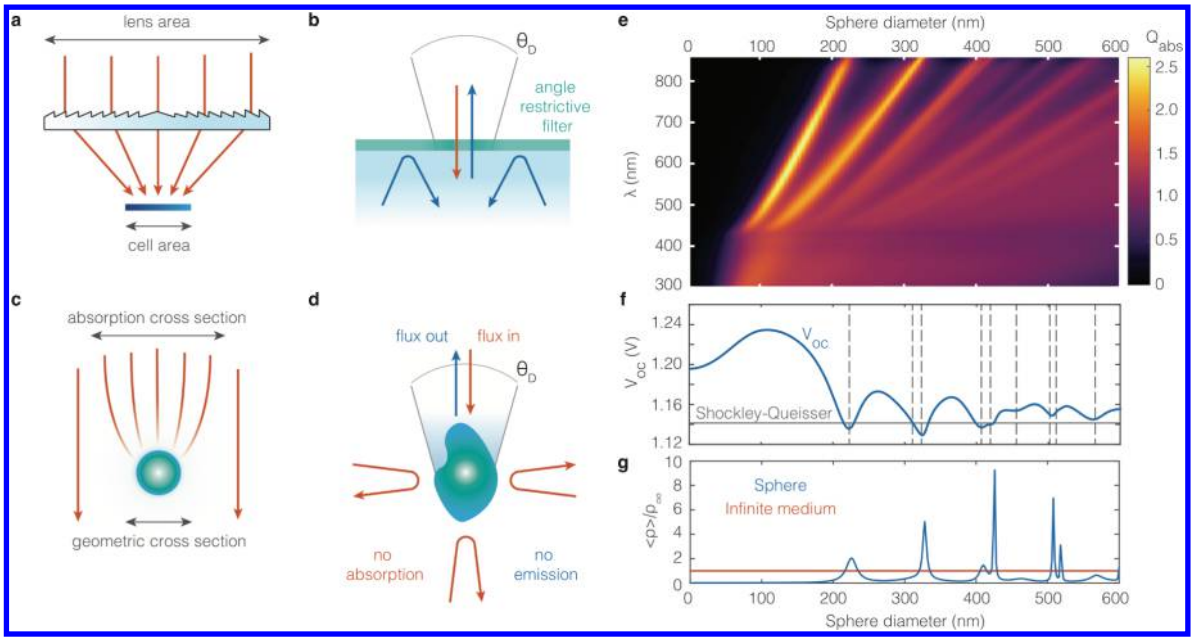

Figure 1. Concentration and large absorption cross sections. (a) Concentrator photovoltaics use a lens to focus light on a small solar cell, thereby enhancing the generation rate of free carriers. (b) In angle restricted photovoltaics, a filter is used to enhance photon recycling and reduce the net recombination rate. (c) Nanostructures can absorb light from an area that is much larger than their own size. (d) Nanostructures can also have anisotropic angular absorption and emission patterns if the structure itself is geometrically asymmetric. (e) Absorption efficiency of a GaAs sphere as a function of photon energy and sphere diameter. (f) Open circuit voltage in the sphere as a function of diameter, which shows clear dips whenever a resonance passes the band gap. Resonant sphere sizes are shown by the vertical dashed lines, in good agreement with dips in the voltage. (g) The local density of states in a sphere with n = 3.64 (representative of GaAs at the band gap) relative to the LDOS in a homogeneous medium with the same refractive index. Whenever a resonance crosses the band gap, there is a significant increase in the LDOS, corresponding to an increase in recombination rates and a decrease in the V_{oc}. The sharp features are not visible in (f) due to averaging over the bandwidth of thermal emission and the presence of losses.

limit, after taking into consideration the difference between geometric and wave optics. We demonstrate this by analyzing the simple case of a GaAs sphere, which has no directivity in absorption, and a single GaAs nanowire, which has weak directivity in absorption. After proving that absorption directivity is required to provide voltage enhancements and larger overall efficiencies, we then discuss the fundamental limitations to directivity using nanostructures and propose two relevant approaches for high directivity. While the role of directivity has been mentioned before,[20] the implications, difficulties, and fundamental limitations of directivity for nanostructured photovoltaics have not yet been discussed. Finally, we discuss the practical implications of how non-radiative recombination in nanoscale systems affects the possibility of enhancing the overall cell efficiency beyond the SQ limit.

RESULTS

Open-Circuit Voltage in Ideal Nanophotonic Systems.

We begin our discussion on ways to achieve voltage enhancement by considering ideal photovoltaic systems, in which the only recombination mechanism is radiative. The open-circuit voltage (V_{oc}) in a solar cell is proportional to the excess carrier density in the active region of the solar cell when no carriers are extracted,[1,23] which is governed by the simple rate equation:

$$G - R_0\frac{n^2}{{n_0}^2} = G - R_0\ \exp\left(\frac{qV_{oc}}{k_BT}\right) = 0 \qquad (1)$$

where G is the generation rate of carriers, n_0 and n are the equilibrium and excess carrier densities, k_B is Boltzman's constant, T is the temperature of the solar cell and ambient (300 K), and q is the electron charge. R_0 is the rate at which the solar cell emits photons when it is in equilibrium with its ambient surroundings (there is no incident sunlight, only blackbody radiation). eq 1 is easily solved for V_{oc}, which leads to the familiar expression:

$$V_{oc} = \frac{k_BT}{q}\ln\left(\frac{G}{R_0}\right) = \frac{k_BT}{q}\ln\left(\frac{I_{sc}}{I_0}\right) \qquad (2)$$

where I_{sc} and I_0 are the short-circuit current and the equilibrium recombination current, respectively.

From eqs 1 and 2, it is clear that the V_{oc} increases if G increases with respect to R_0. This is the mechanism behind the efficiency enhancement in concentrator photovoltaic systems, where the term "concentration" refers to the intensity of incident sunlight. In these systems, a focusing lens enhances the intensity of incident sunlight, which increases the generation rate of carriers (G) but leaves the equilibrium recombination rate (R_0) unchanged. As a result, concentration of incident light directly leads to a larger excess carrier density in the semiconductor and a higher V_{oc}. Semiconductor nanostructures can also concentrate light, based on their nanoantenna functionality of collecting light from a large area and temporarily storing it inside and around the nanostructure (Figure 1c). As a result, the electric-field intensity in the absorbing nanostructure can be orders of magnitude higher than the incident intensity. This similarity has been invoked to suggest that this effect fulfills the same role as macroscopic

DOI: 10.1021/acsnano.6b03950
ACS Nano 2016, 10, 8620−8631

concentration and that nanophotonic solar cells may therefore be intrinsic concentrator solar cells achieving efficiencies above the SQ limit. However, we point out that there is a crucial difference between the two cases: In nanostructures, the enhanced intensity does not lead to a higher carrier density, because the nanoantenna functionality also increases the recombination rate R_0. To understand this, we turn to the expression for R_0 in nanostructured systems in which there is only radiative recombination:

$$R_0 = \int_{E_g/\hbar}^{\infty} \int_0^{\pi} \int_0^{2\pi} \sigma_{abs}(\omega, \theta, \phi)\psi(\omega)\, \sin(\theta) \mathrm{d}\phi \mathrm{d}\theta \mathrm{d}\omega \tag{3}$$

Here E_g is the bandgap energy of the semiconductor, $\hbar$ is the reduced Planck's constant, ω is the optical frequency, $\psi(\omega)$ is the incident blackbody photon flux at 300 K, and σ_{abs} is the absorption cross section as a function of incident angle and frequency. This expression can be found through Kirchhoff's law,[31] which states that an object in thermal equilibrium must emit as many photons as it absorbs. Interaction with the ambient surrounding has no preferred direction, and as a result, eq 3 has to be evaluated over all angles. On the other hand, the generation rate due to the sun only concerns the sun's solid angle (in the absence of diffuse light):

$$G = \int_{E_g/\hbar}^{\infty} \int_0^{\theta_s} \int_0^{2\pi} \sigma_{abs}(\omega, \theta, \phi)S(\omega) \mathrm{d}\phi \mathrm{d}\theta \mathrm{d}\omega \tag{4}$$

where $S(\omega)$ is the AM1.5 solar spectrum[32] and $\theta_s = 0.267°$ is the half angle subtended by the sun. From these equations, it becomes clear that if we increase σ_{abs} over all frequencies and isotropically for all angles of incidence, both G and R_0 will increase by the same amount, implying that the magnitude of σ_{abs} does *not* play a role. The crucial difference between macroscopic and nanophotonic systems, leading to the disparity between concentration and large absorption cross sections, is that lenses necessarily affect the angular response of a solar cell due to conservation of étendue.[33] In fact, we show in Appendix 1 that a concentrating photovoltaic system can be described entirely from the perspective of angle restriction, where the lens is considered an integral part of the photovoltaic system and reduces the equilibrium recombination rate instead of increasing the generation rate. This is very different from nanophotonic systems, which may have large absorption cross sections from all directions.

It turns out that the only way to enable efficiencies above the SQ limit in nanophotonic systems is by reducing the absorption at oblique angles (as shown in Figure 1d), which reduces R_0 but leaves G unchanged. This directivity in absorption is thus similar to angle restriction in macroscopic solar cells[27,29,34] (Figure 1b). It is important to note that, while suppressing σ_{abs} near the band gap can also increase the V_{oc}, this simultaneously comes at a penalty in the short-circuit current. As a result, suppression of absorption cannot be used in a macroscopic device to surpass the Shockley–Queisser efficiency limit,[19] unless when utilizing this effect to construct a multijunction solar cell.[18]

In order to further elucidate the difference between macroscopic and nanophotonic systems, we consider as a basic example a resonant nanosphere that can have large but isotropic absorption cross sections. More specifically, we use eqs 2 and 3 to calculate the generation and recombination rates in a GaAs sphere under solar illumination as a function of sphere diameter. The cross-section σ_{abs}, shown in Figure 1e, is determined using Mie theory.[35] Resonances clearly redshift with increasing radius, eventually passing the band gap of GaAs at 860 nm (top of Figure 1e). Figure 1f shows the corresponding V_{oc} in the sphere, which is strongly modulated by diameter variations, significantly exceeding V_{oc} in a similar Shockley–Queisser type cell (defined by a sharp onset of an isotropic and constant absorption cross section above the band gap). Interestingly, by comparing the two panels, it is easy to verify that these enhancements indeed do not correspond to large absorption cross sections, but actually to the opposite: suppression of absorption near the band gap.[19,23,24,36] This is seen noticing the anticorrelation of the voltage peaks and the absorption resonances moving through the band gap, which has also been observed theoretically for a single nanowire.[17] As we noted before, suppression of absorption near the band gap decreases the equilibrium recombination rate, but cannot lead to efficiencies above the SQ limit in a macroscopic device.

Microscopically, the changes in R_0 are largely due to changes in the local density of optical states (LDOS), which affect the radiative transition rate.[37,38] Figure 1g shows the volume averaged LDOS $\langle\rho\rangle$ in the sphere relative to the LDOS in a homogeneous medium with the same refractive index, $n = 3.64$ (representative of GaAs at the band gap, see Methods for calculation details). When a resonance crosses the band gap, the LDOS is significantly enhanced, which corresponds to increases in the radiative recombination rate and decreases in the V_{oc} (as shown in Figure 1f). Large absorption cross sections are related to LDOS enhancements, and hence by themselves they do not lead to enhanced voltages: the generation and recombination rate are both enhanced, such that the overall effect cancels out.

Directivity in Nanophotonic Structures. The discussion in the previous section has shown that efficiencies above the SQ limit using nanostructures without external concentrating optics can only be achieved by modifying the angular dependence of the absorption pattern: reducing R_0 while maintaining G. This angular anisotropy is captured in the directivity D of the nanostructures, which in antenna theory is commonly used to describe how much power an antenna receives from or transmits into a given solid angle P_Ω, relative to the average power received or transmitted by the antenna in all directions:[39]

$$D = 4\pi P_\Omega / P_{total} \tag{5}$$

It is important to distinguish between directivity in radiation or scattering and directivity in absorption. A simple homogeneous sphere may be moderately directive when it scatters a plane wave or redirects emission from a dipole inside the sphere, sending more light in a certain direction than in others, but it can never be directive in absorption since it looks identical for all directions of incidence. We will elaborate on this distinction later in this article, but for now it is important to keep in mind that the goal is to achieve directivity in absorption.

When the solid angle of maximum absorption directivity is pointed toward the sun, we can use the directivity to derive an expression for the open circuit voltage:

$$V_{oc}(\bar{D}) = V_{oc}^{iso} + \frac{k_B T}{q} \ln(\bar{D}) \tag{6}$$

where

DOI: 10.1021/acsnano.6b03950
ACS Nano 2016, 10, 8620–8631

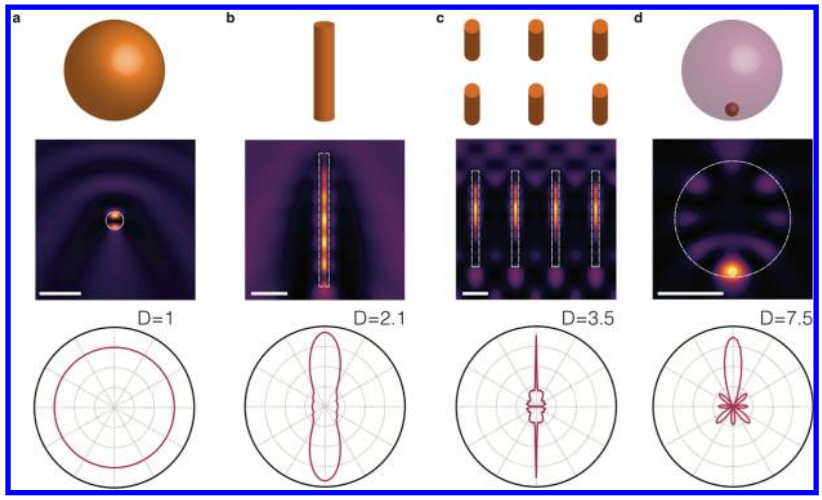

Figure 2. Directivity in nanostructures. (a–d) Schematics showing different nanophotonic structures: a GaAs sphere (a), GaAs nanowire (b), a square array of GaAs nanowires (c), and a lossless sphere with a 40 nm diameter absorbing inclusion asymmetrically embedded in it (d). The top row shows schematic representations of each nanostructure, while the middle row shows the field intensity in the incidence plane, demonstrating the field enhancements corresponding to strong absorption. The corresponding directional absorption is shown in a polar plot in the bottom row, with directivities ranging from a directivity of 1 (no directivity) for the GaAs sphere to a directivity of 7.5 for the lossless sphere with a small absorbing inclusion. The scale bar in each intensity map is 500 nm.

$$\bar{D} = \frac{4\pi \int \psi(\omega)\sigma_{abs}(\omega, \theta = \phi = 0)\mathrm{d}\omega}{\iint \psi(\omega)\sigma_{abs}(\omega, \Omega)\mathrm{d}\Omega\mathrm{d}\omega} \quad (7)$$

Here V_{oc}^{iso} is the open circuit voltage of a nanostructure with isotropic absorption cross section equal to σ_{abs} in the solid angle facing the sun, such as in Figure 1f. Note that $\bar{D}$ is the directivity weighted to the emission spectrum, while D is the directivity at a given frequency, according to eq 5. The weighted directivity $\bar{D}$ reduces R_0 with respect to the isotropic absorber, $R_0 = R_0^{iso}/\bar{D}$, and as such is identical to the restriction factor in conventional angle restriction photovoltaics. Just as with macroscopic angle restriction, directivity is beneficial to the efficiency of a photovoltaic device until absorption within the solid angle subtended by the sun is also reduced. The sun subtends 6.83×10^{-5} sr, resulting in a maximum usable directivity equal to 1.84×10^5 and a voltage increase of 314 mV with respect to an isotropic absorber. In macroscopic angle restriction photovoltaics, the solar cell is planar, extended, and only exposed to a hemisphere, which results in a maximum angle restriction factor of 4.61×10^4 and a maximum voltage increase of 278 mV. It is important to note that the maximum V_{oc} in both cases is the same (when the solid angles of emission and absorption are equal to the solid angle subtended by the sun), but that the V_{oc} without concentration of the nanostructure is lower because it emits into 4π sr.

The absorption directivity of nanostructures strongly depends on their size and shape. Figure 2 shows four examples of nanostructures and their calculated directivity: a simple GaAs sphere, a GaAs nanowire, a nanowire array, and a small lossless sphere with a GaAs inclusion. We have already discussed the GaAs sphere, which can collect light from a large area (Figure 2a, middle) but is fully isotropic (Figure 2a, bottom) and, as a result, cannot lead to efficiencies above the SQ limit. Directivity requires anisotropy in absorptance, which in turn requires an asymmetric shape. In the rest of the paper, we will discuss the other three geometries of Figure 2, which effectively concentrate electric fields (Figure 2b–d, middle row), but, due to their reduced symmetry, can also provide absorption directivity (Figure 2b–d, bottom row).

Single Nanowire. An example of an anisotropic structure that frequently finds use as a nanophotovoltaic element is the nanowire.[40] This geometry has previously been suggested as a candidate for nanophotonic concentration and voltage enhancement because the absorption cross section, when illuminated along the long axis, can be very large due to excitation of weakly confined guided modes at the end facet of the nanowire.[20,21] In addition, when illuminated perpendicular to the nanowire axis, geometrical Mie resonances can be excited,[4,35,41,42] which also lead to significant absorption. Figure 3a shows the calculated open circuit voltage (in black) of a 2 μm long GaAs nanowire as a function of its diameter, when illuminated along the long axis of the nanowire. The V_{oc} is higher than the Shockley–Queisser voltage over almost the entire range of diameters. However, Figure 3a also shows a decomposition of the voltage enhancement into contributions due to absorption directivity and absorption suppression (see Methods for details). From this decomposition, it becomes clear that the gain in voltage is mostly due to suppression of absorption near the band gap, just as with the previous example of the sphere. In fact, for small diameters, the directivity contribution is even negative. This can be understood from Figure 3b, which shows the absorption cross section of the 50 nm diameter GaAs nanowire as a function of incident angle (shown along the polar angle) as well as wavelength (along the radial direction). At normal incidence, absorption rises strongly at 450 nm, but it is very low at longer wavelengths. However, at larger angles and longer wavelengths, the absorption cross section is significantly larger due to excitation of the TM_{01} resonance. As a result, the recombination rate is enhanced with respect to the generation rate, which in turn leads to a voltage decrease instead of a gain.

Directivity does lead to a voltage gain in the nanowire when it has a diameter around 150 nm, as shown in Figure 3a. Figure 3c shows the absorption cross section of the GaAs nanowire for this diameter, showing a strong peak in absorption near the band gap, while absorption at oblique angles is suppressed. This

DOI: 10.1021/acsnano.6b03950
ACS Nano 2016, 10, 8620–8631

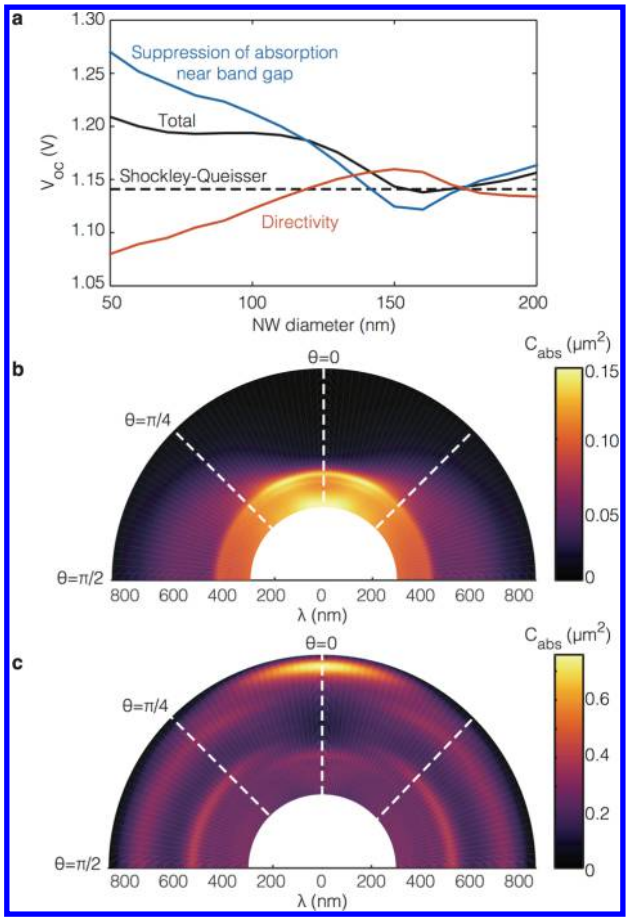

Figure 3. Open circuit voltage in a 2 μm long GaAs nanowire. (a) The V_{oc} of a 2 μm GaAs nanowire as a function of diameter (in black) is significantly larger than the expected Shockley−Queisser V_{oc}. However, when disentangled into the component due to absorption suppression (blue) and higher directivity (red), it turns out that directivity contributes only weakly. (b,c) Absorption spectra as a function of wavelength and incidence angle for 50 (b) and 150 nm (c) diameter, respectively. In the 50 nm diameter wire, absorption due to Mie resonances dominates near the band gap (at $\theta = \pi/2$), while for the 150 nm diameter wire, the HE_{11} guided mode is efficiently excited (at $\theta = 0$).

peak in absorption is due to efficient excitation of the HE_{11} guided mode (note that it is not a resonance[43]), while the suppressed absorption at oblique angles is associated with the fact that the wire coincidentally does not support Mie resonances near the band gap. As a result, the absorption pattern becomes more directive, leading to an increase in the open circuit voltage. The directivity achieved here is about 2.1, which leads to a voltage gain of 19 mV. The fact that voltage enhancements due to concentration are small for nanowires has also been observed in arrays,[44] where detailed balance analysis has shown that InP nanowire arrays do not surpass the regular SQ limit (but only surpass the SQ limit considering a high index passive substrate, which under normal circumstances significantly increases R_0), even though the effective filling fraction is 10 times lower than for the bulk material. Further optimization of the nanowire geometry and interference with the substrate might lead to slightly higher directivities than those observed here,[45] but in the following, we will show that these directivities are much lower than what can be in principle achieved with more suitable nanophotonic structures.

Limits to Directivity. We have discussed in the previous sections how the efficiency enhancement that a nanostructure can achieve is directly related to its maximum absorption directivity. In antenna theory, bounds on directivity have been actively studied for decades in the case of radiation and scattering, and although there is no fundamental limit, there are a few useful practical bounds. These bounds are derived for radiation from an antenna, but they also limit the absorption directivity, and it may therefore be instructive to investigate these bounds and in what regime they apply to absorption.

The optical response of small structures can usually be captured accurately by only a small number of spherical harmonics. This is the basis of Mie theory, which allows the calculation of the scattering and absorption response of canonical objects, such as spheres and infinite cylinders.[35] However, even if the system is not highly symmetric, the scattered and absorbed power of structures with a size on the order of the wavelength can be described accurately as a superposition of only a few scattering harmonics.[46]

The radiation directivity is bounded by the number of spherical harmonics that the structure supports.[47] The radiation patterns associated with the first three spherical harmonics (dipole, quadrupole, and octupole) are shown in Figure 4a (top row). The octupole radiation pattern is the most directive, with a directivity of 4.5. However, by properly combining these harmonics with appropriate relative amplitudes and phases, an even more directive radiation pattern can be obtained. This is shown in the bottom row of Figure 4a: The directivity clearly increases with an increase in the number of harmonics that are supported. This leads to the Harrington limit, which provides the highest possible radiation directivity for a structure that supports up to the Nth spherical harmonic:[47]

$$D_{max}(N) = N^2 + 2N \tag{8}$$

There is also no strict limit on the number of harmonics that can be supported by a structure of a given size, but a useful approximate limit is $N_{max} = nk_0r$, where n is the refractive index of the medium, k_0 is the free space wavevector, and r is the radius of the smallest enclosing sphere. This is equivalent to the number of wavelengths that fit around the circumference of the enclosing sphere. Inserting this into eq 8 leads to the maximum directivity as a function of radius $D_{max}(r) = (nk_0r)^2 + 2nk_0r$, which for large radii is in fact approximately equal to the directivity of a uniformly illuminated circular aperture antenna,[39] $D_{max}(r) \approx (nk_0r)^2$. Higher-order harmonics can be in principle supported by a structure of limited size, but only at the expense of very large Q-factors and sensitivity to losses and disorder.[48] Since here we focus on absorption directivity, the presence of losses is crucial, and superdirective solutions are not feasible.

Figure 4b shows the aperture directivity limit (in blue) as a function of diameter for $n = 3.66$, representative of GaAs near the band gap. This figure also shows the equation for directivity, eq 8, evaluated with the harmonic amplitudes in a GaAs sphere as a function of its diameter. Although a sphere by itself is not directive in absorption, it is instructive to see how many harmonics a known nanophotonic structure supports at these diameters. Interestingly, this curve is significantly lower than the aperture limit, partially because not all harmonics that are supported have the proper amplitude, but also because the highest harmonic supported is actually much lower than $N = nk_0r$. In a GaAs sphere with a diameter of 3 μm and at 860 nm, the highest harmonic with a significant amplitude is $N = 13$,

DOI: 10.1021/acsnano.6b03950
ACS Nano 2016, 10, 8620−8631

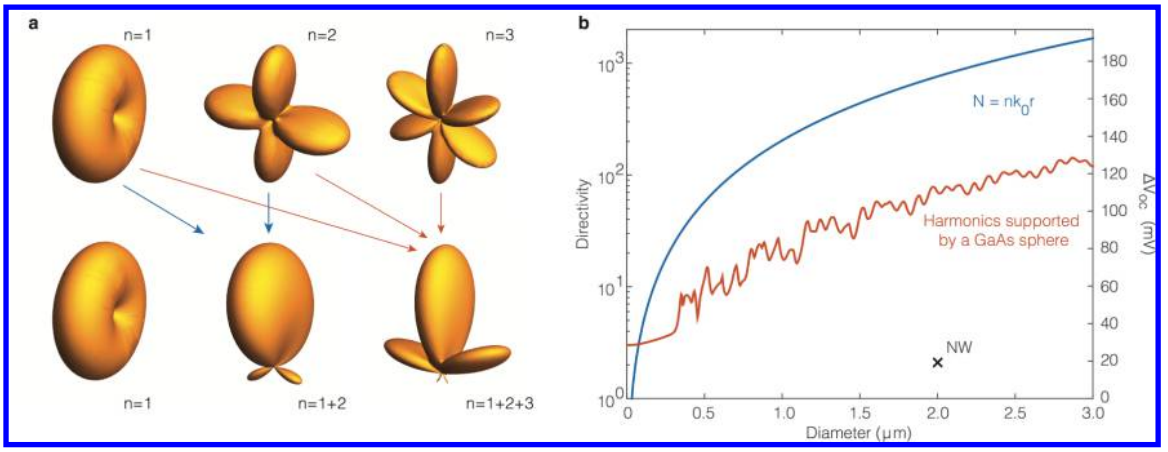

Figure 4. Directivity as a function of spherical harmonics. (a) Radiation patterns of the first three harmonics and increased directivity due to the combination of these spherical harmonics. (b) Maximum directivity as a function of size, assuming that the highest harmonic is given by nk_0r or by taking the amplitudes of the harmonics as in a GaAs sphere at 860 nm. Note that we are only interested in the supported number of harmonics by a physical structure and that the sphere itself is not directive in absorption. The cross depicts the directivity from the nanowire in Figure 3, which is significantly lower than directivities that should in principle be achievable for structures with same size.

while based on the aperture limit one would expect $N = 39$. On the other hand, at very small diameters the nk_0r limit underestimates directivity because the lowest harmonic ($N = 1$) can lead to a radiation directivity of 3 (a so-called Huygens source),[49] and the lowest harmonic has a nonzero amplitude even for very small sizes. If such a directivity of 3 can also be maintained in the absorption pattern over a significant bandwidth (such that $\bar{D} = 3$), this leads to an increase in open circuit voltage of 28.5 mV.

The maximum directivities calculated in Figure 4 are much higher than what we have observed for the single nanowire, whose directivity was at most 2.1 for an object with a "diameter" (longest dimension) of 2 μm (see cross in Figure 4). In contrast, the aperture limit suggests that a directivity of 600 may be achievable, and even the harmonics supported by a sphere imply a directivity that is significantly higher (about 70). It appears that achieving directivity in absorption is much more challenging than in scattering. To understand why, it is instructive to think of a lossless dielectric sphere and a single dipole emitter as an exemplary system. The exact placement and orientation of the emitter in the dielectric antenna yields great control over the excited harmonics, both in their phase and amplitude. With such a single feed point and control over its position and its dielectric environment, directivities close to the Harrington limit can be approached. However, achieving absorption directivity is equivalent to looking for radiation directivity from incoherent sources placed all over the absorptive nanostructure. The fact that these sources are incoherent, and placed over the entire volume, makes achieving high directivity in absorption a significant challenge.

Designing Highly Directive Nanostructures for Absorption. While the Harrington limit may not easily be achieved in an absorbing body, we can still use the limit to gain insight on how to enhance the directivity in absorption. For example, since the limit clearly depends on the effective aperture, a sensible approach to enhance the directivity is to place individual antennas in an array. This approach is already commonly taken to enhance the directivity of small antennas in so-called directional arrays. Hence, to boost the directivity of the individual GaAs nanowire, we also place it into an array (see Figure 2c). This of course largely increases the overall aperture of the absorbing nanostructure, but in any case, the final device layout will require using large arrangements of nanostructures to cover an entire solar cell. In this case, we use the lattice arrangement to maximize absorption directivity, making use of the fact that for certain arrangements and angles of incidence lattice resonances can be excited. These resonances result in strong absorption even at low filling fractions. By tuning the pitch to be close to the wavelength of interest (a pitch of 834 nm), the second-order Bloch mode can be resonantly excited at normal incidence (see Figure 5a at 860 nm and 0°). This leads to a strong directive absorption enhancement at the band edge, which, when averaged over azimuthal angles, gives the absorption/emission pattern shown in Figure 2c. Although absorption at angles close to normal is significantly enhanced, the directivity is still limited to 3.5 (note that since there is no ground plane the array is exposed to free space on both sides). The main reason resides in the strong absorption of sparse nanowire arrays at larger angles,[50] which in this case lies between 10% and 20%, while the absorption at normal incidence peaks at 70%. In contrast, to achieve high directivity, the absorption at off-normal angles needs to be significantly smaller than the peak absorption.

While the directivity of the single nanowire can be enhanced by placing it in an array, the obtained directivity is still small. Suppressing emission and absorption except at specific angles is clearly complicated in nanostructures that completely comprise of an absorbing material. To demonstrate that reducing the absorbing volume can actually increase directivity, we make use of the principle of microscopic reversibility: If it is possible to design a structure that emits directively when excited from a certain feed point in the structure, it is also possible to realize a structure that absorbs in an angularly selective fashion by concentrating the loss at that feed point. For very small lossy inclusions, the absorption directivity approaches the radiation directivity from an unpolarized feed point at the same location.

We explore a spherical nonabsorbing antenna (refractive index $n = 2$) which is driven by spontaneous emission from a small amount of absorbing material inside the sphere ($n = 2 + 2i$, Figure 2d). The spherical harmonics are now only excited efficiently with amplitudes and phases fixed by the location of the inclusion, which can lead to much increased directivity (Figure 5b), in this case up to $D = 7.5$. A simple way to understand this is by looking at the absorption of the structure

DOI: 10.1021/acsnano.6b03950
ACS Nano 2016, 10, 8620–8631

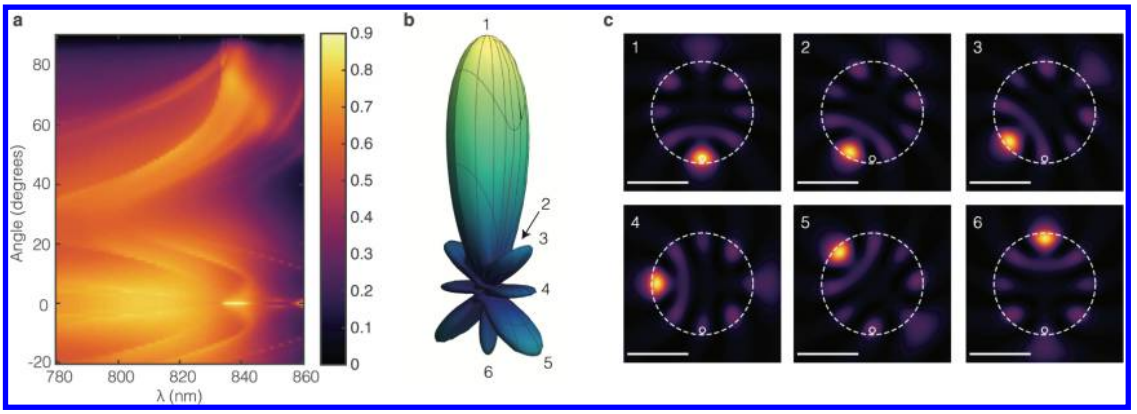

Figure 5. Designs for high directivity. (a) Absorption of unpolarized light in a square array of nanowires with 834 nm pitch as a function of angle and wavelength for 2 μm long GaAs nanowires with a diameter of 150 nm. Excitation of Bloch modes is clearly visible. (b) Emission/absorption pattern at λ = 860 nm from a 906 nm diameter sphere with n = 2, with a 60 nm diameter lossy inclusion (n = 2 + 2i) located at 412 nm from the center of the sphere. (c) The electric-field intensity inside the sphere due to plane wave illumination as a function of incident angle, corresponding to the numerals in (b). The peak in absorption/emission occurs when the hot spot overlaps with the lossy inclusion, and consecutive peaks and dips in emission correspond to peaks and dips in the intensity distribution. The scale bar is 500 nm.

when it is driven by a plane wave. For this specific size (907 nm diameter), there is a large hot spot in the sphere, at the position where we place the lossy inclusion (Figure 5c). In this case, the hot spot overlaps with the lossy inclusion, and the absorption is strong. However, if we change the angle of incidence, the hot spot rotates along the sphere and moves away from the lossy inclusion, which reduces the absorptance. Hence, the peaks and nodes in the directivity pattern correspond to the intensity maxima and minima in the sphere overlapping with the inclusion, as shown in Figure 5b,c.

Practical Implications for Nanophotonic Solar Cells. Although the nanowire array and spherical lossy inclusion that we explored in the previous section may achieve enhanced directivity, they are not yet practical designs to achieve efficiencies above the Shockley−Queisser limit in macroscopic solar cells. Both designs suffer from low short-circuit current due to the low filling fraction of absorbing material. However, in principle, directivity and large currents can be obtained at the same time, allowing for efficiencies above the Shockley−Queisser limit. This property requires designing a solar cell that achieves strong absorption between the band gap of the semiconductor and the shortest wavelength in the solar spectrum, but that at the same time is very directive in the narrow region near the band gap that is dominated by emission (a width larger than k_BT/q, about 26 mV). For example, an efficient directive GaAs solar cell needs to absorb all of the incident sunlight between 300 and 860 nm to achieve high current, while simultaneously being directive between about 800 and 860 nm.

The importance of maintaining high J_{sc} is evident from Figure 6a, which shows the efficiency relative to the SQ limit for a GaAs solar cell as a function of its J_{sc} (relative to the maximum current) and directivity. Because the efficiency depends logarithmically on the directivity but linearly on the J_{sc}, small penalties in the current reduce the overall device efficiency to below the SQ limit even at reasonable directivities. For example, a weighted directivity of 10 only leads to efficiencies above the SQ limit if the J_{sc} remains above 95%. So far we have not yet demonstrated a peak directivity of 10 even in poorly absorbing structures, highlighting how challenging it may be to achieve both goals simultaneously. However, as is clear from Figure 4, this outstanding design challenge may well be worth the effort since significant enhancements in V_{oc} can be expected. Based on our analysis, it appears that the best approach to enhance intrinsic directivity in a nanophotonic solar cell is to combine an absorber with a nonabsorbing nanostructured host material that enhances directivity, as in Figure 2d. Such an arrangement has already been investigated to enhance absorption in small lossy nanostructures[51,52] and would also be similar to the usual arrangement of an angle restriction solar cell, where a multilayer structure is placed on top of the absorber.[27,28] However, these multilayer structures are required to be many microns thick to achieve significant directivity, and simultaneously achieving broadband transmission over the whole wavelength range is very challenging.[27] Hence, it is worthwhile to investigate additional approaches to angle restriction.

It is important to stress that the previous considerations hold for materials strongly dominated by radiative recombination. However, many materials appropriate for photovoltaic purposes have significant nonradiative recombination. In the presence of nonradiative recombination, the total recombination current increases:[53,54]

$$R_0^{\text{total}} = R_0\left(\frac{\eta_{\text{int}}p_{\text{esc}}}{1-\eta_{\text{int}}p_{\text{abs}}}\right)^{-1} = R_0\left(\frac{\Gamma_r p_{\text{esc}}}{\Gamma_{\text{nr}} + (1-p_{\text{abs}})\Gamma_r}\right)^{-1} \quad (9)$$

where p_{esc} and p_{abs} are the reabsorption and escape probability of radiative recombination events in the semiconductor averaged over the semiconductor volume, $\eta_{int} = \Gamma_{rad}/(\Gamma_{rad} + \Gamma_{nrad})$ is the internal quantum efficiency, and Γ_{rad} and Γ_{nrad} are the radiative and nonradiative recombination rates. The term in parentheses in eq 9 is known as the external radiative efficiency (η_{ext}), and it directly reduces the open-circuit voltage: $V_{oc} = V_{oc}^{rad} + k_BT/q\ln(\eta_{ext})$. In the following we assume that there is no parasitic absorption, such that $p_{esc} = 1 - p_{abs}$.

In the traditional approach to angle restriction, which relies on external multilayer structures, the angle restriction factor and photon escape probabilities are intrinsically linked due to conservation of momentum along the multilayer interfaces. From Snell's law, one can show that the probability that a photon escapes a sufficiently thin solar cell with ideal back reflector is given by

DOI: 10.1021/acsnano.6b03950
ACS Nano 2016, 10, 8620−8631

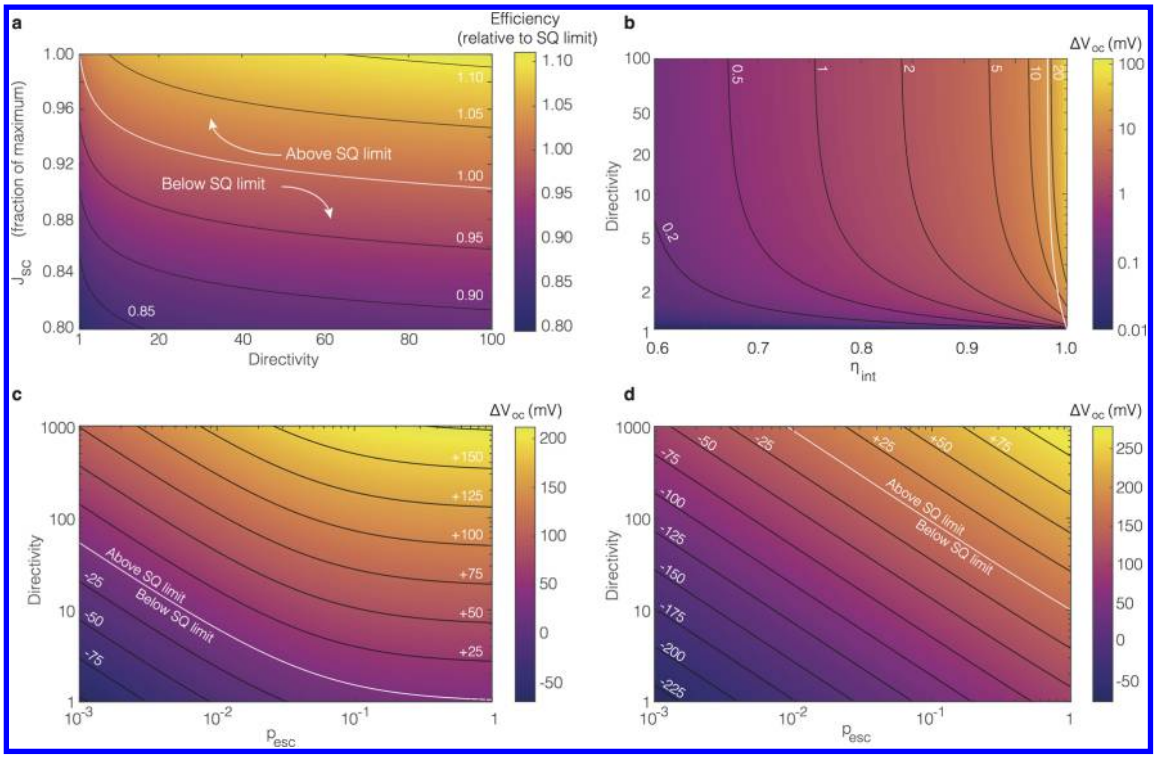

Figure 6. Practical implications for high-directivity designs. (a) The color map shows the efficiency of a GaAs solar cell as a function of its directivity and fraction of maximum current. With maximum current and no directivity, the solar cell reaches the SQ limit, and with increased directivity at no cost in current, the solar cell beats the SQ limit. However, at very small penalties in J_{sc} the solar cell will already perform below the SQ limit, even for reasonable directivities. This indicates the importance of maintaining high currents, when trying to achieve directivity. (b) The color map and black contour lines show the V_{oc} gain due to directivity as a function of the semiconductor internal quantum efficiency (η_{int} for planar angle restriction systems, with respect to no angle restriction). To the right of the white contour line, the SQ limit is surpassed. (c,d) The color maps show the gain in V_{oc} for different combinations of p_{esc} and $\bar{D}$ with respect to a planar cell with $p_{esc} = 1/2n^2$ and $\bar{D} = 1$, for (c) GaAs ($\eta_{int} = 0.95$) and (d) Si or CIGS ($\eta_{int} = 0.01$), respectively. The contour lines in both figures are now not related to the color maps, but show the absolute distance in V_{oc} to the SQ limit, highlighting that in both cases the SQ limit can still be broken.

$$p_{esc} = \frac{\Omega_c}{2\pi} = 1 - \sqrt{1 - \sin^2(\theta_D)/n^2} \approx \frac{\sin^2(\theta_D)}{2n^2} \qquad (10)$$

where Ω_c is the solid angle subtended by the critical angle in the substrate and θ_D is the angle to which emission is limited by the angle restriction filter. Eq 10 gives an upper limit to the escape probability for planar solar cells, which is achieved only if the cell is sufficiently thin (such that $\alpha d \ll 1$, where α is the absorption coefficient and d is the thickness of the active layer). See, *e.g.*, refs 53, 55, and 28 for a discussion of escape probabilities in the presence of larger αd.

By restricting the emission angle, the escape probability decreases simultaneously, due to the fact that the critical angle decreases. In fact, if η_{int} is sufficiently low (such that $\eta_{ext} \approx \eta_{int} p_{esc}$), the decrease in R_0 and p_{esc} due to angle restriction cancels out completely.[28,56] This is clearly visible in Figure 6b, where the color map shows the gain in V_{oc} due to angle restriction, relative to a planar cell with the same η_{int} but no directivity. Even for η_{int} as high as 0.6, the enhanced directivity and reduced p_{esc} still cancel out, with only negligible V_{oc} enhancements of $\Delta V_{oc} < 1$ mV. To achieve voltage enhancements larger than 10 mV, an η_{int} of at least 93% is required, which so far only GaAs has achieved.[55] In fact, due to the high rate of photon recycling, even small amounts of nonradiative recombination lead to large voltage drops when compared to ideal materials: For a directivity of 10, an η_{int} of 95% reduces the open-circuit voltage by 69 mV, and at a directivity of 100, the voltage drop is 127 mV (ref 57). To surpass the SQ limit with a planar angle restriction system (shown by the white contour line in Figure 6b), $\eta_{int} > 0.96$ is required. Note that this is an optimiztic scenario for planar films; in real systems where $\alpha d \approx 1$ the requirement on η_{int} is even more stringent.

To reap the benefits of directivity, the relationship between the photon escape probability and directivity thus has to be broken. This is automatically done in nanostructures, where the absence of planar interfaces relaxes the constraints placed by momentum conservation along the interfaces on the escape probability. If directivity and the photon escape probability are uncorrelated, significant increases can be achieved in the open circuit voltage even in the presence of nonradiative recombination. This is shown in Figure 6c,d for $\eta_{int} = 0.95$ and $\eta_{int} = 10^{-2}$, which are η_{int} representative of the best GaAs (6c) and Si and CIGS (6d) solar cells, respectively.[58] These color maps show the increase in V_{oc} relative to a planar cell with escape probability $1/2n^2$. Clearly, for both values of η_{int} significant increases in V_{oc} with respect to the planar reference case can be achieved by enhancing simultaneously the directivity and photon escape probability. Superimposed on these color maps are contour lines that show the absolute difference in V_{oc} to the SQ limit, highlighting that the SQ limit can still be surpassed as long as both p_{esc} and the directivity are sufficiently enhanced. In general, from eq 9, one can derive the lowest η_{int} for which the SQ limit can still be beaten given a combination of directivity and p_{esc}:

DOI: 10.1021/acsnano.6b03950
ACS Nano 2016, 10, 8620–8631

$$\eta_{int} > (1 - (1 - \bar{D})p_{esc})^{-1} \quad (11)$$

From Figure 6d, it is apparent that, even for low η_{int}, increases in directivity and p_{esc} both contribute to enhanced V_{oc}, as long as an increase in one parameter does not come at the expense of the other parameter.

The photon escape probability can also be increased in planar angle restriction solar cells by texturing the back surface, as discussed in the Supporting Information of ref 28. However, utilizing nanostructures to enhance directivity and p_{esc} may have additional benefits. For example, nanophotonics offers control over the LDOS, which means that the radiative recombination rate Γ_{rad} and thus η_{int} itself can be increased. Additionally, through control over the LDOS, light trapping can also be enhanced even beyond the $1/4n^2$ limit.[7,15] As a result, the total number of bulk defect centers in the solar cell can be reduced by reducing the amount of bulk material, without sacrificing current. If simultaneously the surface recombination velocity does not increase, Γ_{nrad} decreases, and the η_{int} increases again.[59,60] This means that, even if the degree of directivity attainable in broadband absorbing nanostructures is limited, these nanostructures can perhaps be used to enhance η_{ext} in conjunction with *e.g.*, concentrating lenses, angle restriction filters,[27−29,61,62] or even external cavities[28,30,63] to achieve directivity. However, in the latter two, external approaches care must be taken not to reduce p_{esc} too much, or the benefit of nanostructuring is undone.

CONCLUSIONS

In this paper we have discussed efficiency enhancement above the Shockley−Queisser limit using nanophotonic principles. We showed that the increase in absorption cross section available in nanoparticles cannot help break the Shockley−Queisser limit, but that increased directivity in absorption can provide such an efficiency gain. Achieving directivity in a small absorbing nanostructure is challenging, and it requires careful engineering. Fruitful ways to achieve directivity in actual nanophotonic solar cells may be to use arrays or combinations of absorbing and lossless nanostructures. However, while designing a directive solar cell, care should be taken that the penalty in short-circuit current is minimal. Furthermore, in the presence of nonradiative recombination, efficiencies above the Shockley−Queisser limit can still be realized as long as both the directivity and photon escape probabilities are enhanced. These photon escape probability enhancements are additive to traditional voltage enhancement strategies, such as concentrating lenses, which make nanostructuring a powerful approach even in combination with other more traditional schemes.

METHODS

The calculations for the sphere were performed using Mie theory,[35] except for the sphere LDOS calculations. LDOS calculations rely on evaluating the imaginary part of the Green's dyadic, $\mathrm{Im}(\vec{\mathbf{G}}(\mathbf{r}, \mathbf{r}))$, at the source location, which we averaged over the sphere volume:

$$\frac{\langle \rho \rangle}{\rho_\infty} = \frac{6\pi}{Vk} \int \frac{1}{3} \mathrm{Tr}(\mathrm{Im}(\vec{\mathbf{G}}(\mathbf{r}, \mathbf{r}))) \mathrm{d}\mathbf{r} \quad (12)$$

Here V is the sphere volume, and we take the trace of the Green's dyadic to account for dipole orientation, and we used the fact that the homogeneous Green's dyadic evaluates to $\mathrm{Im}(\vec{\mathbf{G}}_0(\mathbf{r}, \mathbf{r})) = \mathbf{I}k/6\pi$ (where $\mathbf{I}$ is the identity matrix and k is the wavenumber in the medium). Ref 64 gives convenient formulas for normalized transition rates of dipoles located inside a sphere, which readily enable evaluation of eq 12.

Figure 3a shows disentanglement of the contributions to the V_{oc} due to suppression or enhancement of absorption near the band gap and due to the angular distribution of the absorption cross section. To distinguish between the different contributions, we first calculate the total "concentration factor":

$$X = \frac{4\pi \int \psi(\omega) H(\omega - \omega_{bg}) \mathrm{d}\omega}{\iint \psi(\omega) \sigma_{abs}(\omega, \Omega) \mathrm{d}\Omega \mathrm{d}\omega} \quad (13)$$

where $H(\omega - \omega_{bg})$ is the Heaviside step-function with onset at the band gap frequency ω_{bg} and $\psi(\omega)$ is the blackbody spectrum at ambient temperatures. The numerator with the Heaviside step-function is thus proportional to the standard isotropic Shockley−Queisser emission rate, while the denominator is proportional to the actual emission rate. The ratio of the two rates naturally gives the enhancement factor. We can rewrite eq 13 as

$$X = \frac{\int \psi(\omega) H(\omega - \omega_{bg}) \mathrm{d}\omega}{\int \psi(\omega) \sigma_{abs}(\omega, \theta = \phi = 0) \mathrm{d}\omega} \times \frac{4\pi \int \psi(\omega) \sigma_{abs}(\omega, \theta = \phi = 0) \mathrm{d}\omega}{\iint \psi(\omega) \sigma_{abs}(\omega, \Omega) \mathrm{d}\Omega \mathrm{d}\omega} \quad (14)$$

where now the first term only corresponds to the spectral shape of σ_{abs}, but σ_{abs} is assumed to be isotropic, while the second term captures the contribution of the angle dependence of σ_{abs}. The first term gives the enhancement factor due to suppression of emission near the band gap, A, while second term indeed corresponds to $\bar{D}$ as given by eq 7. To calculate the contributions to the voltage explicitly, we use

$$\Delta V_{oc} = \frac{k_B T}{q} \ln(X) = \frac{k_B T}{q} (\ln(A) + \ln(\bar{D})) = \Delta V_{oc}^A + \Delta V_{oc}^D \quad (15)$$

where ΔV_{oc}^A and ΔV_{oc}^D are the contributions to the V_{oc} due to the absorption edge and directivity, respectively.

The simulations for the single nanowire and lossy inclusion were performed with Lumerical FDTD,[65] and the simulations of the array of nanowires were performed using S^4, a free package for the Fourier modal method.[66]

APPENDIX A

Equivalence of Angle Restriction and Concentration

It is instructive to take a closer look at concentration and angle restriction in macroscopic photovoltaic systems, to further elucidate why large absorption cross sections are not necessarily comparable to concentration. The limiting efficiency of a photovoltaic device can be calculated by considering fluxes entering and exiting the solar cell, where the solar cell itself is considered a "black box" with a given absorptance and quantum efficiency. It should not matter whether we consider a flux surface just above the solar cell or above the concentrator lens, in which case the lens is considered an integral part of the solar cell and resides inside the black box. However, this leads to an apparent paradox: The intensity of sunlight incident on the solar cell is much higher than the one incident on the lens, yet in both cases we should find the same increase in V_{oc}. This paradox is resolved by considering the angular response of the lens/solar cell system, as shown in Figure A1. If we consider the lens as an active part of the photovoltaic system, the generation rate per unit area is identical to that of a regular solar cell without a lens, but the recombination rate is strongly affected by the presence of the lens. For flat, extended systems, eq 3 becomes[1,23]

DOI: 10.1021/acsnano.6b03950
ACS Nano 2016, 10, 8620−8631

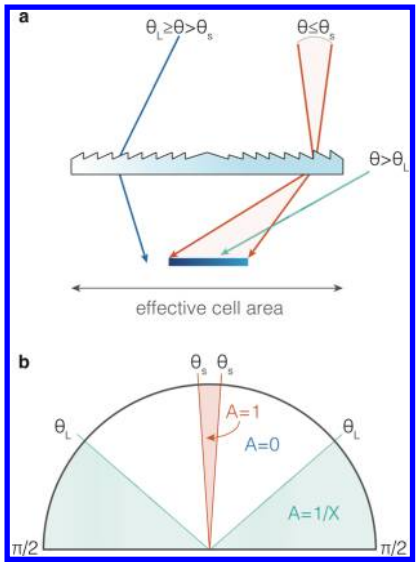

Figure A1. Equivalence of angle restriction and concentration. (a) A lens also acts as an angular filter for a solar cell, which only transmits light into the solar cell that is incident within the solid angle of the sun, while light that is incident with larger angles is focused next to the solar cell. Light incident at very oblique angles still hits the solar cell, but with lower intensity. (b) Polar plot representation of the absorptance of an ideal solar cell when considering the lens as an integral part of the system. The lens has a concentration factor of X. The red shading indicates the solid angle of solar illumination (exaggerated for visibility), the green shade indicates angles for which light directly illuminates the solar cell without passing the lens, and the white shade indicates angles for which the solar cell is missed completely.

$$R_0 = \int_{E_g/\hbar}^{\infty}\int_0^{\pi}\int_0^{\pi/2} A(\omega, \theta, \phi)\Theta(\omega)\,\sin(\theta)\,\cos(\theta)\mathrm{d}\phi\mathrm{d}\theta\mathrm{d}\omega \tag{A1}$$

where the $\cos(\theta)$ is the lambertian and $A(\omega, \theta, \phi)$ is the absorptance. From Figure A1, it is clear that for certain angles ($\theta_s < \theta \leq \theta_L$, where θ_L is the angle of the edge of the lens to the edge of the cell), black-body radiation does not generate carriers in the semiconductor at all, because the action of the lens directs the radiation next to the solar cell. At very large angles the solar cell is directly exposed to black-body radiation, but because it doesn't pass the lens the intensity is lower by a factor X, where the concentration factor of the lens is given by $X = \sin^2(\theta_L)/\sin^2(\theta_s)$. If we evaluate eq A1 according to Figure A1, we find

$$R_0^L = \pi\left(\sin^2(\theta_s) + \frac{1}{X}\cos^2(\theta_L)\right)\int_{E_g/\hbar}^{\infty}\Theta(\omega)\mathrm{d}\omega \tag{A2}$$

When comparing this to the recombination rate of a solar cell without a concentrating lens to find the angle restriction enhancement factor X_{AR}, we find

$$X_{AR} = \left(\sin^2(\theta_s) + \frac{1}{X}\cos^2(\theta_L)\right)^{-1} = X \tag{A3}$$

where we used the expression for X given above. Hence, as one would expect, the voltage enhancement due to a lens can be described both from the perspective of concentration and angle restriction, and both lead to the same result. This even holds in the presence of non-radiative recombination: A lens does not affect the escape probability or internal quantum efficiency, and as a result η_{ext} is independent of the concentration factor X. The total recombination rate given in eq 9, therefore, still scales with $1/X$. Note that in practice, a lens and an angle restriction filter block different angles, and they can, therefore, be used in conjunction with additive voltage enhancements, as long as the angle restriction filter does not block angles incident from the lens.[56]

AUTHOR INFORMATION

Corresponding Author

*E-mail: garnett@amolf.nl.

Present Address

[‖]Department of Electrical and Systems Engineering, University of Pennsylvania, 220 South 33rd Street, Philadelphia, PA 19104-6314, United States

Notes

The authors declare no competing financial interest.

ACKNOWLEDGMENTS

We are grateful to E. Alarcon-Llado for feedback on the manuscript. This work is part of the research program of FOM, which is financially supported by The Netherlands Organization for Scientific Research (NWO). S.A.M. and E.C.G. were also supported by funding from the European Research Council under the European Union's Seventh Framework Programme ((FP/2007-2013)/ERC grant agreement no. 337328, "Nano-EnabledPV"). A.A. acknowledges a fellowship of the Royal Netherlands Academy of Sciences (KNAW), support from the Air Force Office of Scientific Research, the Welch Foundation (grant No. F-1802), and the Simons Foundation.

REFERENCES

(1) Shockley, W.; Queisser, H. J. Detailed Balance Limit of Efficiency of P-N Junction Solar Cells. *J. Appl. Phys.* **1961**, *32*, 510−519.
(2) Brongersma, M. L.; Cui, Y.; Fan, S. Light Management for Photovoltaics Using High-Index Nanostructures. *Nat. Mater.* **2014**, *13*, 451−460.
(3) Ferry, V. E.; Verschuuren, M. A.; Li, H. B. T.; Verhagen, E.; Walters, R. J.; Schropp, R. E. I.; Atwater, H. A.; Polman, A. Light Trapping in Ultrathin Plasmonic Solar Cells. *Opt. Express* **2010**, *18*, A237.
(4) Mann, S. A.; Grote, R. R.; Osgood, R. M.; Schuller, J. A. Dielectric Particle and Void Resonators for Thin Film Solar Cell Textures. *Opt. Express* **2011**, *19*, 25729.
(5) Mann, S. A.; Garnett, E. C. Extreme Light Absorption in Thin Semiconductor Films Wrapped around Metal Nanowires. *Nano Lett.* **2013**, *13*, 3173−3178.
(6) Grote, R. R.; Brown, S. J.; Driscoll, J. B.; Osgood, R. M.; Schuller, J. A. Morphology-Dependent Light Trapping in Thin-Film Organic Solar Cells. *Opt. Express* **2013**, *21*, A847.
(7) Callahan, D. M.; Munday, J. N.; Atwater, H. a. Solar Cell Light Trapping beyond the Ray Optic Limit. *Nano Lett.* **2012**, *12*, 214−218.
(8) Ulbrich, C.; Fahr, S.; Üpping, J.; Peters, M.; Kirchartz, T.; Rockstuhl, C.; Wehrspohn, R.; Gombert, A.; Lederer, F.; Rau, U. Directional Selectivity and Ultra-Light-Trapping in Solar Cells. *Phys. Status Solidi A* **2008**, *205*, 2831−2843.
(9) Garnett, E.; Yang, P. Light Trapping in Silicon Nanowire Solar Cells. *Nano Lett.* **2010**, *10*, 1082−1087.
(10) Wallentin, J.; Anttu, N.; Asoli, D.; Huffman, M.; Aberg, I.; Magnusson, M. H.; Siefer, G.; Fuss-Kailuweit, P.; Dimroth, F.; Witzigmann, B.; Xu, H. Q.; Samuelson, L.; Deppert, K.; Borgström, M. T. InP Nanowire Array Solar Cells Achieving 13.8% Efficiency by Exceeding the Ray Optics Limit. *Science* **2013**, *339*, 1057−1060.

DOI: 10.1021/acsnano.6b03950
ACS Nano 2016, 10, 8620−8631

(11) Beck, F. J.; Mokkapati, S.; Catchpole, K. R. Plasmonic Light-Trapping for Si Solar Cells Using Self-Assembled, Ag Nanoparticles. *Prog. Photovoltaics* **2010**, *18*, 500−504.
(12) Pala, R. A.; Liu, J. S. Q.; Barnard, E. S.; Askarov, D.; Garnett, E. C.; Fan, S.; Brongersma, M. L. Optimization of Non-Periodic Plasmonic Light-Trapping Layers for Thin-Film Solar Cells. *Nat. Commun.* **2013**, *4*, 2095.
(13) Tan, H.; Santbergen, R.; Smets, A. H. M.; Zeman, M. Plasmonic Light Trapping in Thin-Film Silicon Solar Cells with Improved Self-Assembled Silver Nanoparticles. *Nano Lett.* **2012**, *12*, 4070−4076.
(14) Atwater, H. A.; Polman, A. Plasmonics for Improved Photovoltaic Devices. *Nat. Mater.* **2010**, *9*, 205−213.
(15) Yu, Z.; Raman, A.; Fan, S. Fundamental Limit of Nanophotonic Light Trapping in Solar Cells. *Proc. Natl. Acad. Sci. U. S. A.* **2010**, *107*, 17491−17496.
(16) Polman, A.; Atwater, H. A. Photonic Design Principles for Ultrahigh-Efficiency Photovoltaics. *Nat. Mater.* **2012**, *11*, 174−177.
(17) Sandhu, S.; Yu, Z.; Fan, S. Detailed Balance Analysis and Enhancement of Open-Circuit Voltage in Single-Nanowire Solar Cells. *Nano Lett.* **2014**, *14*, 1011−1015.
(18) Yu, Z.; Sandhu, S.; Fan, S. Efficiency above the Shockley−Queisser Limit by Using Nanophotonic Effects To Create Multiple Effective Bandgaps With a Single Semiconductor. *Nano Lett.* **2014**, *14*, 66−70.
(19) Munday, J. N. The Effect of Photonic Bandgap Materials on the Shockley−Queisser Limit. *J. Appl. Phys.* **2012**, *112*, 064501.
(20) Xu, Y.; Gong, T.; Munday, J. N. The Generalized Shockley−Queisser Limit for Nanostructured Solar Cells. *Sci. Rep.* **2015**, *5*, 13536.
(21) Krogstrup, P.; Jørgensen, H. I.; Heiss, M.; Demichel, O.; Holm, J. V.; Aagesen, M.; Nygard, J.; Fontcuberta i Morral, A. Single-Nanowire Solar Cells beyond the Shockley−Queisser Limit. *Nat. Photonics* **2013**, *7*, 306−310.
(22) Niv, A.; Gharghi, M.; Gladden, C.; Miller, O. D.; Zhang, X. Near-Field Electromagnetic Theory for Thin Solar Cells. *Phys. Rev. Lett.* **2012**, *109*, 138701.
(23) Sandhu, S.; Yu, Z.; Fan, S. Detailed Balance Analysis of Nanophotonic Solar Cells. *Opt. Express* **2013**, *21*, 1209−1217.
(24) Mann, S. A.; Garnett, E. C. Resonant Nanophotonic Spectrum Splitting for Ultrathin Multijunction Solar Cells. *ACS Photonics* **2015**, *2*, 816−821.
(25) Dorodnyy, A.; Alarcon-Lladó, E.; Shklover, V.; Hafner, C.; Fontcuberta i Morral, A.; Leuthold, J. Efficient Multiterminal Spectrum Splitting via a Nanowire Array Solar Cell. *ACS Photonics* **2015**, *2*, 1284−1288.
(26) Rau, U.; Paetzold, U. W.; Kirchartz, T. Thermodynamics of Light Management in Photovoltaic Devices. *Phys. Rev. B: Condens. Matter Mater. Phys.* **2014**, *90*, 35211.
(27) Kosten, E. D.; Kayes, B. M.; Atwater, H. A. Experimental Demonstration of Enhanced Photon Recycling in Angle-Restricted GaAs Solar Cells. *Energy Environ. Sci.* **2014**, *7*, 1907.
(28) Kosten, E. D.; Atwater, J. H.; Parsons, J.; Polman, A.; Atwater, H. A. Highly Efficient GaAs Solar Cells by Limiting Light Emission Angle. *Light: Sci. Appl.* **2013**, *2*, e45.
(29) Höhn, O.; Kraus, T.; Bauhuis, G.; Schwarz, U. T.; Bläsi, B. Maximal Power Output by Solar Cells with Angular Confinement. *Opt. Express* **2014**, *22*, A715−722.
(30) Braun, A.; Katz, E. A.; Feuermann, D.; Kayes, B. M.; Gordon, J. M. Photovoltaic Performance Enhancement by External Recycling of Photon Emission. *Energy Environ. Sci.* **2013**, *6*, 1499.
(31) Landau, L. D.; Lifshitz, E. M. *Electrodynamics of Continuous Media*; Pergamon Press: Oxford, U.K., 1960; Vol. *8*.
(32) NREL. *Air Mass 1.5 (AM1.5) Global Spectrum (ASTM173−03G)*; http://rredc.nrel.gov/solar/spectra/am1.5/ (accessed August 30, 2016).
(33) Sala, G.; Antón, I. Photovoltaic Concentrators. In *Handbook of Photovoltaic Science and Engineering*; John Wiley & Sons, Ltd: Chichester, U.K., 2011; pp 402−451.
(34) Araújo, G. L.; Martí, A. Absolute Limiting Efficiencies for Photovoltaic Energy Conversion. *Sol. Energy Mater. Sol. Cells* **1994**, *33*, 213−240.
(35) Bohren, C. E.; Huffman, D. R. *Absorption and Scattering of Light by Small Particles*; John Wiley & Sons, Inc.: New York, 1983.
(36) Niv, a.; Abrams, Z. R.; Gharghi, M.; Gladden, C.; Zhang, X. Overcoming the Bandgap Limitation on Solar Cell Materials. *Appl. Phys. Lett.* **2012**, *100*, 083901.
(37) Zambrana-Puyalto, X.; Bonod, N. Purcell Factor of Spherical Mie Resonators. *Phys. Rev. B: Condens. Matter Mater. Phys.* **2015**, *91*, 195422.
(38) Novotny, L.; Hecht, B. *Principles of Nano-Optics*; 2nd ed.; Camrbidge University Press: New York, 2012.
(39) Balanis, C. E. *Antenna Theory: Analysis and Design*, 3rd ed.; John Wiley & Sons, Inc.: Hoboken, NJ, 2005.
(40) Garnett, E. C.; Brongersma, M. L.; Cui, Y.; McGehee, M. D. Nanowire Solar Cells. *Annu. Rev. Mater. Res.* **2011**, *41*, 269−295.
(41) Cao, L.; White, J. S.; Park, J.-S.; Schuller, J. a; Clemens, B. M.; Brongersma, M. L. Engineering Light Absorption in Semiconductor Nanowire Devices. *Nat. Mater.* **2009**, *8*, 643−647.
(42) Abujetas, D. R.; Paniagua-Domínguez, R.; Sánchez-Gil, J. a. Unraveling the Janus Role of Mie Resonances and Leaky/Guided Modes in Semiconductor Nanowire Absorption for Enhanced Light Harvesting. *ACS Photonics* **2015**, *2*, 921−929.
(43) Anttu, N.; Xu, H. Q. Efficient Light Management in Vertical Nanowire Arrays for Photovoltaics. *Opt. Express* **2013**, *21*, A558−575.
(44) Anttu, N. Shockley−Queisser Detailed Balance Efficiency Limit for Nanowire Solar Cells. *ACS Photonics* **2015**, *2*, 446−453.
(45) van Dam, D.; Abujetas, D. R.; Paniagua-Domínguez, R.; Sánchez-Gil, J. A.; Bakkers, E. P. A. M.; Haverkort, J. E. M.; Gómez Rivas, J. Directional and Polarized Emission from Nanowire Arrays. *Nano Lett.* **2015**, *15*, 4557−4563.
(46) Ruan, Z.; Fan, S. Temporal Coupled-Mode Theory for Light Scattering by an Arbitrarily Shaped Object Supporting a Single Resonance. *Phys. Rev. A: At., Mol., Opt. Phys.* **2012**, *85*, 43828.
(47) Harrington, R. F. Effect of Antenna Size on Gain, Bandwidth, and Efficiency. *J. Res. Natl. Bur. Stand. - D. Radio Propag.* **1960**, *64D*, 1−12.
(48) Alu, A.; Engheta, N. Enhanced Directivity From Subwavelength Infrared/Optical Nano-Antennas Loaded With Plasmonic Materials or Metamaterials. *IEEE Trans. Antennas Propag.* **2007**, *55*, 3027−3039.
(49) Hansen, J. E. *Spherical Near-Field Antenna Measurements*; Peter Peregrinus, Ltd.: London, 1988.
(50) Grzela, G.; Paniagua-Domínguez, R.; Barten, T.; van Dam, D.; Sánchez-Gil, J. A.; Rivas, J. G. Nanowire Antenna Absorption Probed with Time-Reversed Fourier Microscopy. *Nano Lett.* **2014**, *14*, 3227−3234.
(51) Khudiyev, T.; Bayindir, M. Superenhancers: Novel Opportunities for Nanowire Optoelectronics. *Sci. Rep.* **2014**, *4*, 7505.
(52) Yu, Y.; Ferry, V. E.; Alivisatos, a P.; Cao, L. Dielectric Core−Shell Optical Antennas for Strong Solar Absorption Enhancement. *Nano Lett.* **2012**, *12*, 3674−3681.
(53) Steiner, M. A.; Geisz, J. F.; García, I.; Friedman, D. J.; Duda, A.; Kurtz, S. R. Optical Enhancement of the Open-Circuit Voltage in High Quality GaAs Solar Cells. *J. Appl. Phys.* **2013**, *113*, 123109.
(54) Ganapati, V.; Steiner, M. A.; Yablonovitch, E. The Voltage Boost Enabled by Luminescence Extraction in Solar Cells. *IEEE J. Photovoltaics* **2016**, *6*, 801−809.
(55) Schnitzer, I.; Yablonovitch, E.; Caneau, C.; Gmitter, T. J. Ultrahigh Spontaneous Emission Quantum Efficiency, 99.7% Internally and 72% Externally, from AlGaAs/GaAs/AlGaAs Double Heterostructures. *Appl. Phys. Lett.* **1993**, *62*, 131−133.
(56) Martí, A.; Balenzategui, J. L.; Reyna, R. F. Photon Recycling and Shockley's Diode Equation. *J. Appl. Phys.* **1997**, *82*, 4067.
(57) Miller, O. D.; Yablonovitch, E.; Kurtz, S. R. Strong Internal and External Luminescence as Solar Cells Approach the Shockley−Queisser Limit. *IEEE J. Photovoltaics* **2012**, *2*, 303−311.
(58) Green, M. A. Radiative Efficiency of State-of-the-Art Photovoltaic Cells. *Prog. Photovoltaics* **2012**, *20*, 472−476.

DOI: 10.1021/acsnano.6b03950
ACS Nano 2016, 10, 8620−8631

(59) Campbell, P.; Green, M. A. The Limiting Efficiency of Silicon Solar Cells under Concentrated Sunlight. *IEEE Trans. Electron Devices* **1986**, *33*, 234−239.
(60) Tiedje, T.; Yablonovitch, E.; Cody, G. D.; Brooks, B. G. Limiting Efficiency of Silicon Solar Cells. *IEEE Trans. Electron Devices* **1984**, *31*, 711−716.
(61) Shen, Y.; Ye, D.; Celanovic, I.; Johnson, S. G.; Joannopoulos, J. D.; Soljačić, M. Optical Broadband Angular Selectivity. *Science* **2014**, *343*, 1499−1501.
(62) Shen, Y.; Hsu, C. W.; Yeng, Y. X.; Joannopoulos, J. D.; Soljačić, M. Broadband Angular Selectivity of Light at the Nanoscale: Progress. *Appl. Phys. Rev.* **2016**, *3*, 011103.
(63) van Dijk, L.; van de Groep, J.; Di Vece, M.; Schropp, R. E. I. Exploration of External Light Trapping for Photovoltaic Modules. *Opt. Express* **2016**, *24*, A1158.
(64) Chew, H. Transition Rates of Atoms near Spherical Surfaces. *J. Chem. Phys.* **1987**, *87*, 1355.
(65) Lumerical Solutions, Inc. *FDTD Solutions*; http://www.lumerical.com/tcad-products/fdtd/ (accessed August 30, 2016).
(66) Liu, V.; Fan, S. S4: A Free Electromagnetic Solver for Layered Periodic Structures. *Comput. Phys. Commun.* **2012**, *183*, 2233−2244.

DOI: 10.1021/acsnano.6b03950
ACS Nano 2016, 10, 8620−8631